Viscosity variability impact on 2D laminar and turbulent Poiseuille velocity profiles; Characteristic-Based Split (CBS) stabilization

Antonio Pasculli
Dept. of Engineering Geology (INGEO)
and
Member of the INDAM Research group GNCS (National Institute of Advanced Mathematics; National Group of Scientific Computing)
University G. D'Annunzio
Chieti-Pescara, Italy
a.pasculli@unich.it

***Abstract*—The erosion of riverbeds and riverbanks depends, among other causes, both on the velocity fields and on their gradient near their boundaries, with the generation of shear stresses. The presence of sediments modifies the viscosity and, accordingly, modifies the profiles, particularly near the edges right where they are generated. Therefore, in this work, the distortion of the velocity profiles due to an imposed spatial variability of viscosity, was studied applying the *Computational Fluid Dynamics* (CFD). In particular, as test cases, laminar and turbulent *Plane Poiseuille flows*, were selected. For simplicity, it was assumed that the sediment distribution and therefore the viscosity distribution was not influenced by the mixing due to velocity field. That is, the equilibrium configuration was determined as a consequence of a spatially variable distribution of viscosity. The 2D Navier-Stokes equations, in steady state conditions, were numerically solved exploiting a research software developed and discussed by the author [1]. The turbulence was considered through the RANS (Reynolds Averaged Navier Stokes) approach. The two equations $k-\varepsilon$ *models* were employed. The turbulence phenomena near solid boundaries was simulated by the means of *Wall-Functions*. Spatial discretization was carried out using the *Finite Element Method* (FEM). A structured meshing with *h* like adaptability was developed. Then, in order to avoid velocities and pressure instabilities, the *Characteristic-based split algorithm* (CBS) was applied, while, in order to correctly consider incompressibility, by a numerical point of view, the *Method of Artificial Compressibility* (AC) was selected. Accordingly, the related CBS-AC *three steps algorithm* was implemented [1]. Then, some parametric numerical experiments were performed, considering a semi-implicit, approach. As was to be expected, the velocity profiles, for both laminar and turbulent were influenced by the viscosity distribution. The discussion of the overall results points out the sensitivity of the algorithms not only to the meshes size, to their distribution and to the number of iterations, but also to some intrinsic "experimental numerical dials" (safe coefficients, explicit vs implicit ratio), specific of the selected approach. Moreover, suggestions have emerged for more complex and more complete simulations which, necessarily, would use methods based on iterations internal to each time-step**

Keywords*—*Navier-Stokes equations; CBS stabilization; RANS turbulence; FEM; variable viscosity

I. INTRODUCTION

Erosion and sediment transport occurrences involve multiple interactions among fluid flow, particles, moving boundaries, geotechnical characteristics of riverbanks and riverbed and much more. Among many others, one issue is the numerical solution of the differential equations related to the selected models. The most general and 'ab initio' commonly exploited approach is based on the *Balance Equations* of physics, pursued by the *Computational Fluid Dynamic* (CFD). Namely, Navier-Stokes and Newton's laws equations have to be solved [2] supplemented by experimental laws that define the parameters related to the mass transport of material, the rate of erosion, (e.g. [3], among many others), the *constitutive-laws,* etc. The phenomena complexity implies, necessarily, a splitting of the modelling in two or more different spatial scales: macro scales of many meters wide or more, and smaller scales of few centimeters wide or less. The *Reduced Complexity Models* (RCM), to which *Cellular Automata* (CA) approach belongs [4], represents an important alternative to the CFD, in particular in order to predict morphological changes, within large spatial area, for example within fluvial dynamic at reach [5, 6] and at catchment scale [7], and over relevant time scale (climate evolution as well). This kind of modelling approach could be a suitable tool also within the framework of the landslides susceptibility maps construction and in the study of morphology variations of a territory [8, 9]. Moreover, frequent wetting and drying phenomena, induced also by rainfall variability due to, in particular, climate change, may lower soil mechanical strength (for example for pyroclastic soils [10, 11]), triggering possible landslides occurrences. Also in this case the CA approach may be useful in order to evaluate sediment production and transport. Very accurate local calculation, at small scale, based necessarily on CFD, beside a stochastically determination of mechanical parameters [12, 13], could be used in order to construct 'experimental-numerical laws' to be introduced in simplified models like *Shallow Water*, CA or others approaches. The discretization of the spatial domain is commonly achieved through not only structured or unstructured meshing, but also by *mesh-less* approaches, which avoid the construction of meshes, like *Smoothed Particle Hydrodynamics* (SPH) [14, 15]. Turbulence is an important phenomenon, not completely understood by physical, mathematical and numerical points of view. By the numerical viewpoint, the most accurate approach is the *Direct Numerical Simulation* (DNS) of fluid and particles flows [16, 17]. On the other hand, its application on large or medium scales is not very practical due to very high CPU time and memory requested for high and either medium Reynolds number. Representation of the solution by a less expansive approach, *Large-Eddy Simulation* (LES) has been investigated by many authors. But LES is still subject to severe constraints when wall bounded flows are considered, because (at least theoretically) the internal region of the

978-1-5386-7500-7/19/$31.00 ©2019 IEEE
DOI 10.1109/MCSI.2018.00038

boundary layer needs to be quasi-directly resolved, yielding large computational costs. DNS and/or LES could be used in small localized subdomains where an accurate description of the flow is requested, while computing the rest of the configuration by means of a less-accurate method that, in any case, should be linked to the other regions. By consequence, to pursue the purpose of this paper, the 2D *Reynolds Averaged Numerical Simulation* (RANS), $k-\varepsilon$ two-equations turbulence closure models (Launder & Jones, [18]) implemented in [1], were selected.

II. 2D MATHEMATICAL MODELLING

The simulations described in this work were carried out using the research code developed by the author and described in [1] and based on the numerical solution of 5 equations: one related to *mass conservation*; two related to *momentum balance* along horizontal (x) and vertical (y) coordinates; one related to *production, diffusion and transport* of turbulent kinetic energy, while the last one related to *dissipation* of the *turbulent energy*. A brief and overall description of the main contents of the selected models is given below.

A. Mass conservation

In Einstein summation convention:

$$\frac{\partial \rho}{\partial t}+\frac{\partial(\rho u_i)}{\partial x_i}=0 \quad i=1,2 \tag{1}$$

where ρ is the water-sediments volumetric mass density, assumed, for simplicity, constant and equal to 10^3 Kg/m^3; u_i the i^{th} velocity component.

B. Momentum balance (Navier Stokes Equations)

In order to build constitutive laws related to viscous fluids the *strain temporal rates tensor* $\dot{\varepsilon}_{ij}$, related to small deformation, was introduced. Then relations between the *strain tensor* and the *stress tensor*, for *linear Newtonian and isentropic fluids,* were provided: $\tau_{ij}=2\mu\dot{\varepsilon}_{ij}-\delta_{ij}\dot{\varepsilon}_{kk}$, while the v*olume viscosity* was neglected. In the *turbulent regime* flow, a further stress term, due to *turbulent kinetic energy k*, should be introduced $\tau_{ij}^t=\mu_t\frac{\partial u_i}{\partial x_j}-\rho k$ where ρ is the *volumetric density*, μ_t is the turbulent dynamic viscosity which will be described in following paragraphs, while k [m]^2[s]$^{-2}$ is the half of the *turbulent square velocity* $=(1/2)(u_x'^2+u_y'^2)$ where $u_x'^2, u_y'^2$ are *velocities fluctuation,* μ is the *laminar dynamic viscosity*. Thus:

$$\frac{\partial \rho u_i}{\partial t}+\frac{\partial[(\rho u_j)\cdot u_i]}{\partial x_j}-\frac{\partial(\tau_{ij}+\tau_{ij}^t)}{\partial x_j}+\frac{\partial p}{\partial x_i}-\rho g_i=0 \tag{2}$$

$$i=1,2\ ;\quad j=1,2$$

where p is the pressure [Pa], g is the gravity acceleration.

C. Turbulent modelling

Among others, the RANS (Reynolds Averaged Navier Stokes) *two equations* $k-\varepsilon$ model with the 2D *Wall-Functions* proposed by Fan et al. [19], were implemented.

D. Production and transport equation of the turbulent kinetic energy

By means of the *general scalar conservation equation*, the following relation was considered:

$$\frac{\partial \rho k}{\partial t}+\frac{\partial[(\rho u_i)k]}{\partial x_i}-\frac{\partial}{\partial x_i}\left[(\mu+\frac{\mu_t}{\sigma_k})\frac{\partial k}{\partial x_i}\right]+(P+G-\rho\varepsilon)=0 \tag{3}$$

where $\mu_t=\rho C_\mu f_\mu\left(k^2/\varepsilon\right)$ is the turbulent viscosity; C_μ an experimental parameter (see below); f_μ a factor included into the *Wall Functions* (for details see [1]); ε [m]^2[s]$^{-3}$ the volumetric *density rate dissipation of the turbulent Kinetic energy*; $P=\mu_t\left\{2\cdot\left[\left(\frac{\partial u_x}{\partial x}\right)^2+\left(\frac{\partial u_y}{\partial y}\right)^2\right]+\left(\frac{\partial u_x}{\partial x}+\frac{\partial u_y}{\partial y}\right)^2\right\}$ is the source of the *turbulent kinetic energy* due to the s*hearing stress*; G the turbulence source due to *buoyancy forces*, if any.

E. Production and transport equation of the dissipation rate of the turbulent kinetic energy.

By means of the same approaches adopted in the previous section:

$$\frac{\partial \rho\varepsilon}{\partial t}+\frac{\partial[(\rho u_i)\cdot\varepsilon]}{\partial x_i}-\frac{\partial}{\partial x_i}\left[(\mu+\frac{\mu_t}{\sigma_\varepsilon})\frac{\partial \varepsilon}{\partial x_i}\right]+\frac{\varepsilon}{k}(C_{\varepsilon 1}f_{\varepsilon 1}P+ C_{\varepsilon 1}G-C_{\varepsilon 2}f_{\varepsilon 2}\rho\varepsilon)=0 \tag{4}$$

where the value of the parameters are specified in the following subsection.

F. Experimental parameters

For these kind of turbulence models it was necessary to calibrate the mathematical equations with experimental parameters. In this paper the following values were selected [20]: $C_\mu=0.09$; $C_{\varepsilon 1}=1.44$, $C_{\varepsilon 2}=1.44$; $\sigma_t=0.9$; $\sigma_k=1.$; $\sigma_\varepsilon=1.3$.

G. Wall Functions

In order to introduce the weakening of the turbulence close to rigid boundaries, valid for low-Reynolds number and for steady turbulent boundary layers flow, the *Wall Functions* proposed by Fan were adopted ([1] and [19]).

H. Boundaries conditions related to turbulence modelling

Along rigid boundaries, the turbulent kinetic energy was assumed to be zero, while its dissipation on boundary elements was assumed to be $\varepsilon_w=2\nu\left(\frac{\partial k^{0.5}}{\partial n}\right)^2$, where n is the normal direction. At the inlet flow, it was assumed: $k=0.05\times\sqrt{u_x^2+u_y^2}$.

III. NUMERICAL MODELLING

The application of the *Finite Element Standard (FEM) Galerkin Methods*, in order to solve numerically the previous equations, implies *instabilities* in particular for *convective mode predominance* respect to *diffusive mode*. Furthermore *incompressibility* causes *pressure instabilities*. Thus to avoid velocities and pressure instabilities the *Characteristic-based split algorithm* (CBS) and the *Method of Artificial compressibility* (AC) [20] were, respectively, applied. For the transient, *dual time stepping* method may be adopted with *Internal-External Local Time Stepping*. The CBS based on *Artificial compressibility* (AC) or the CBS-AC method, despite other methods proposed in literature, consists in only three steps:

Step 1 Momentum equation without pressure terms:

$$\Delta U_i^* = \Delta t\left[-\frac{\partial(u_j U_i)}{\partial x_j}+\frac{\partial(\tau_{ij}+\tau_{ij}^t)}{\partial x_j}+(\rho g_i)+ +\frac{\Delta t}{2}u_k\frac{\partial}{\partial x_k}\left(\frac{\partial(u_j U_i)}{\partial x_j}-\rho g_i\right)\right]^n \tag{5}$$

where $U_i=\rho u_i$ is the flux vector, $\Delta t = saf\cdot f(Peclet)$ is the time step calculated as a function of local Peclet number (see below) and *saf* a safety coefficient to assure the convergence;

Step 2 Pressure calculation from Poisson equation:

$$\Delta\rho=\left(\frac{1}{c^2}\right)^n\Delta p=-\Delta t\left[\frac{\partial U_i^n}{\partial x_i}+\theta_1\frac{\partial\Delta U_i^*}{\partial x_i}-\Delta t\theta_1\left(\frac{\partial^2 p^n}{\partial x_i\partial x_i}+\theta_2\frac{\partial^2\Delta p}{\partial x_i\partial x_i}\right)\right] \tag{6}$$

for which the θ Wilson procedure (also called β Method, [2] pag. 72) was adopted.

Step 3 Velocity correction:

$$\Delta U_i^{**}=-\Delta t\frac{\partial p^{n+\theta_2}}{\partial x_i}+\frac{\Delta t^2}{2}u_k^n\frac{\partial}{\partial x_k}\left(\frac{\partial p^n}{\partial x_i}\right) \tag{7}$$

The flux value, calculated at time step 1, is corrected: $U_i^{n+1}=U_i^n+\Delta U_i^*+\Delta U_i^{**}$, so at the end of the *(n+1)*-th time step: $u_i^{n+1}=U_i^{n+1}/\rho$. *The most important advantage of this procedure is the possibility to implement arbitrary order for the velocity and the pressure interpolation without an artificial damping. In this way the necessity to satisfy the heavy Babuska-Brezzi condition* is avoided. Important consequences of the selected approach (for more details pages. 273-283 [2]) are: a *more simplicity and reliability* of the implementation process; *very fast algorithm* for *non-high Mach* number flow, with very good precision. By these three steps, fluid-dynamic fields (velocity and pressure) were evaluated. The momentum equations are *nonlinear* due to convective terms. Thus to linearize the system, the velocity product of the convective terms were assumed to be formed by the value of the velocity evaluated at the previous step, calculated as an *average within the local element* (Gauss point) and the updated value of the velocity. Further details, related to the selection of *artificial compressibility*, *dual time stepping*, *matrix inversion* and *lumping*, were given in [1]. Some important parameters had to be correctly tuned to reach convergence of the iterative procedure. It is well known that in convective predominance flux, in order to avoid instabilities, the time step should assume optimal values (*Petrov Galerkin*), function of *Peclet number* $Pe=(u\cdot h)/2k$ where u is the velocity, h the mesh characteristic size and k is the diffusion parameter (thermal or mass diffusion, kinematic viscosity etc.). *Peclet number depends on local conditions*. *Thus a nodal time step was introduced by the evaluation of the minimum time step for each node*. Moreover, in order to ensure the stabilization of nonlinear terms [1], a *safety coefficient* (*saf*) had to be introduced that further decreases the *internal time step* (on which the temporal stability depends) and also the *external time step* (which provides the stabilization of the spatial approximations) [2]. In order to perform some testing and comparison with simplified turbulence models, in [1] and in this paper, the outcomes of the selected turbulence model obtained by turbulent Poiseuille test have been compared with the *Prandtl's Mixing Length Theory* and *Deissler's sublayer and buffer zones* models [21]. However, more recently, an interesting analytical models were proposed, [22, 23, 24, 25], which fit very well both some experimental data and Direct Numerical Simulations (DNS) results.

IV. NUMERICAL TESTS

Among available fluid dynamical analytical tests, designed to check the correctness of numerical algorithms, the *Plane Poiseuille Problem,* consisting of two horizontal indefinite parallel planes, 0.5 m far away to each other and 1. m long, through which a stream of water flows, characterized by a maximum speed of 1 m/s, was selected. Initially, the water flow was supposed to be clear, without sediments, so: $\rho=10^3[\text{kg}][\text{m}]^{-3}$ and $\mu=97.8\times10^{-5}[\text{Pa}][\text{s}]$. The inlet velocity profile of the *x* component was assumed parabolic along *y*, while the *y* component was assumed to be zero. Initially, the velocity was zero everywhere, except at the inlet. *No slip condition* (zero velocities) was assumed on the two horizontal boundaries. At the inlet the pressure was imposed to be $p[\text{Pa}]=9.8\cdot10^4+8.\mu L$ (according to the theory [20]), where L was the length of the strip (thus $p[\text{Pa}]=9.8\cdot10^4+0.007824$) while, initially, in any other points the pressure was set equal to $9.8\cdot10^4$ [Pa]. Then, some numerical experiments were carried out assuming a sediment distribution along the direction perpendicular to the mean flow velocity, affecting only the laminar term of the viscosity, excluding, for the sake of simplicity, its influence on the turbulent part. Further in order to identify more clearly how a viscosity variability (due to sediment concentration variability) along the vertical coordinates *y* may affect the shape of the *x* velocity profile, the hydrostatic pressure was excluded. According to these assumptions the pressure resulted to be constant on planes perpendicular to flow vector (*y* direction) and linearly decreasing along the longitudinal coordinate. In all the performed calculations, an uniform or clustered *structured meshing,* obtained by 18 up to 22 nodes along the *y* direction and up to 43 nodes along the longitudinal *x* direction, for a maximum, respectively, of 967 nodes and 1806 elements, were selected. In all the elaborations carried out in this paper, the following parameters, according to [1] and [2] (pag. 72), were adopted: *Wilson's coefficients* $\theta_1=1.$, $\theta_2=1.$; *reference velocity* (AC model) = 1 m/s, advised for high Reynolds

number, but assumed to be suitable also in the cases studied in this paper. Then, the influence on the numerical results of the nonuniform grid was explored, introducing the following coordinates transforming algorithm (pag. 544 [2]):

$$y' = H \cdot \frac{(2\alpha+\beta)\cdot\left(\frac{\beta+1}{\beta-1}\right)^{\frac{y-\alpha}{1-\alpha}} + 2\alpha - \beta}{(2\alpha+1)\left[\left(\frac{\beta+1}{\beta-1}\right)^{\frac{y-\alpha}{1-\alpha}} + 1\right]} \qquad (8)$$

where y and y' are nodes ordinates, respectively, before and after the transformation. If the length L, x and x' nodes abscissas are considered instead of, respectively, the height H and the nodes ordinates, the mesh clustering of the inlet and outlet vertical boundaries are obtained. The elements clustering density depends on two parameters, $0 < \alpha$ and $1 < \beta < \infty$, which must be selected. In Fig. 1 the plots of two meshing realizations, both with $\alpha = 0.5$ and $\beta = 1.15$, are reported. In the following two sub-sections, the testing of the developed algorithms are briefly detailed, regarding both laminar and turbulent flows.

A. Laminar Poiseuille flow

The numerical approach described in sections II and III, requires an iterative procedure. In [1] results obtained by 500 iterations, adopting only horizontal boundaries mesh clustering (Fig. 1a), were discussed first of all. The velocity profiles resulting from numerical calculations showed a general good behaviour compared to analytical solution, easily available in literature. However, the analysis revealed a substantial difference (about 30%) among numerical and analytical values of the velocities just along the boundaries where the results, for erosion phenomena elaboration, should be more accurate. Nevertheless, it was reached an almost perfect symmetry (within the 10th decimal digit) respect to the longitudinal axes, due to the symmetry of the grid, not obtainable with a different spatial covering strategy also if through the same type of element. The pressure profile was very satisfactory and uniform (0.45% maximum relative error) showing, anyway, the same numerical qualitative trend of the velocities profiles.

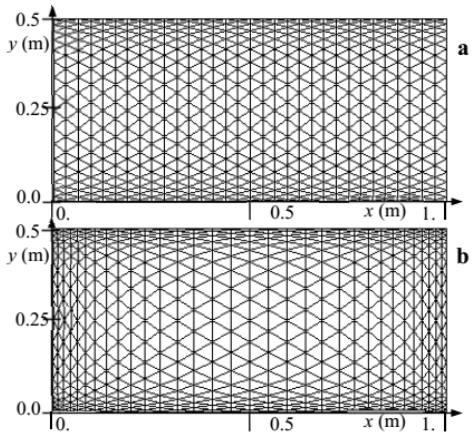

Fig.1. Adaptative meshing: a) only horizontal boundaries mesh clustering; b) clustering of all boundaries (freely adapted from [1]).

By consequence it was necessary to increment the number of iterations. Fig. 2 (from [1]) reports the results obtained after 2000 iterative steps. The overall numerical results for both velocities (0.9% as maximum relative error) and pressure (0.08%) were very satisfactory.

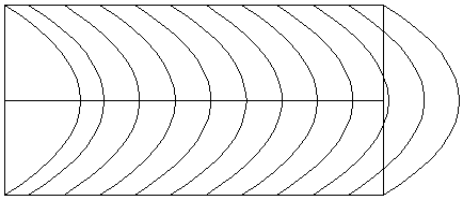

Fig. 2. Laminar Poiseuille test; total velocity profiles after 2000 iterations, top and bottom boundaries meshing clustering, Fig. 1b (from [1]).

Furthermore other not reported plots show that the calculated numerical vertical component velocities, provided by the solution of the related 2D numerical algorithms (theoretically zero), did not exceed 10^{-5}m/s.

B. Turbulent Poiseuille flow

For the *turbulent plane Poiseuille* problem, the following parameters were selected: *safety coefficient*=0.2; *pressure stability coefficient* (rateo between internal and external time step)=2. In particular, to obtain the convergence, it was necessary to drastically lower the *safety coefficient* from 0.9 (laminar flow) down to 0.2. Figs. 3a, b and c show the *averaged velocities* profile, obtained with only top and bottom boundaries meshes clustering with $\alpha = 0.5$ and $\beta = 1.15$.

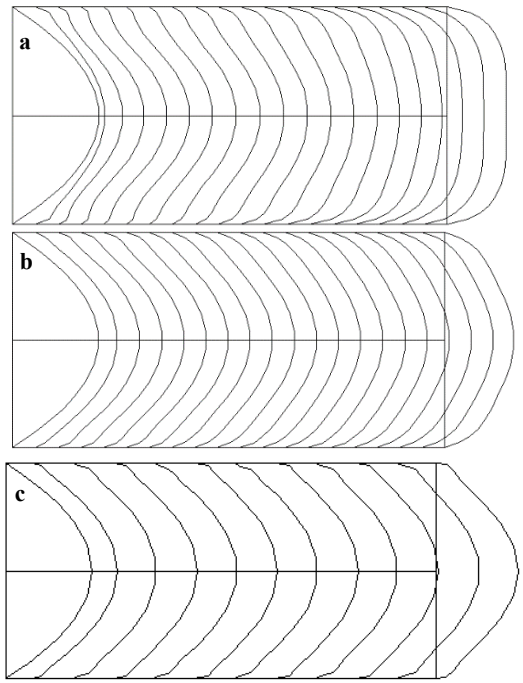

Fig. 3. Turbulent Poiseuille test, lumping matrix, only up and down boundaries meshes clustering, total velocity profiles after: a) 500 iterations; b) 800 iterations; c) 3000 iterations; (plot c from [1]).

Moreover, notwithstanding it was applied a simplified inversion technique (lumping matrix), faster than the classical approach, satisfactory results were obtained. The figure show how the velocity profiles change their distribution as the iterations number increases. In particular as the simulations carried out through 3000 iterations (Fig. 3c) clearly shows, it is possible to highlight the capability of these kind of algorithm to forecast the occurrence of a thin boundary layer, within which a strong velocity variation and for this reason a strong shear stresses occur.

C. *Numerical-Analytical Turbulent Poiseuille problem comparison*

In order to make some comparisons with simplified turbulence models, the *Prandtl's Mixing Length Theory* and *Deissler's sublayer and buffer zones* models ([21], pp. 149-161) were selected. The comparisons were necessarily semi-quantitative since different assumptions underlay each models. Dimensionless parameters were introduced: $u^+ = u/u*$ is the dimensionless velocity, where u is, in this case, the longitudinal u_x velocity; $u* = \sqrt{\tau_0/\rho}$ is the reference velocity, while $\tau_0 = \mu \frac{du_x}{dy}$ is the shear stress at the wall; $y^+ = y \cdot (u* \rho)/\mu$ the dimensionless distance from the wall. In Prandtl-Deissler approach the turbulence region is divided into three main areas: viscous or laminar sub-layer $0 \le y^+ < 5$; buffer layer $5 \le y^+ < 26$; turbulent core $26 \le y^+$. For each area, separate equations yield. Within the turbulent core, Prandtl introduced the logarithmic velocity distribution which can be rearranged in the following dimensionless form: $u^+ = \left(ln\, y^+ \right)/0.36 + 3.8$. The numerical values were suggested by Deissler, by the means of experimental considerations. Efforts have been made to reduce the number of equations by combining the sublayer and buffer zones. Deissler, assuming an exponential form of the eddy viscosity, suggested the following integral equation, where n is an experimental parameter fitting (for Fig. 5 n=0.124 was selected) :

$$u^+ = \int_0^{y^+} \frac{dy^+}{1 + n^2 u^+ y^+ \left[1 - exp\left(-n^2 u^+ y^+\right)\right]} \qquad (9)$$

Equation (9) was solved by a numerical iteration methods, whose algorithm has not been reported in this paper. Each integration was realized by three Gauss points approach. In Fig. 4a and b two different simulations are reported, related to turbulent flow and total boundaries meshes clustering. It is worth noting that, as expected, the velocity profiles were influenced also by the selected clustering parameters. Then, analytical values were compared to the numerical results carried out with clustered meshing, obtained with $\beta = 1.15$ and $\beta = 1.01$, through 3000 iterations (Fig. 4b). The last β value allowed a finer meshing along the longitudinal boundaries. Fig. 5 is related to analytical and numerical distribution velocities calculated at the section 0.865 [m] far from the inlet, with the meshes clustering adopted to obtain Fig. 4b. In addition, the parabolic inlet velocity was also considered for the purpose of comparison. As Fig. 5 shows, the match between numerical and analytical results are satisfactory within the viscous layer, while in the other zones the comparison is not well enough, requiring a better spatial domain discretization.

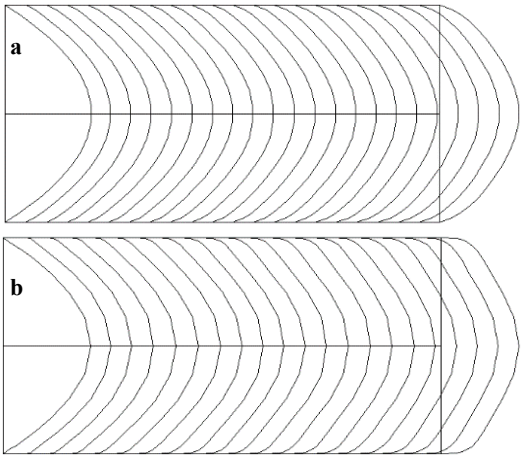

Fig. 4. Turbulent Poiseuille test, total velocity profiles after 3000 iterations, lumping matrix, total boundaries meshes clustering a) $\alpha = 0.5$, $\beta = 1.15$; b) $\alpha = 0.5$, $\beta = 1.01$.

V. NUMERICAL EXPERIMENTS ASSUMING A VARIABLE SEDIMENT AND VISCOSITY DISTRIBUTION

In order to analyse, by a parametric approach, the influence of variable sediment distributions on the calculated velocity profile of the flow, the following relation ([26]) was selected:

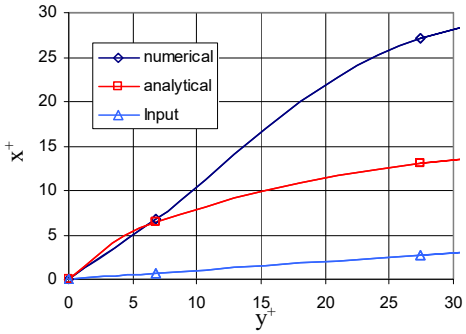

Fig. 5. Analytical, numerical and input turbulent velocities profile comparison, related to Fig. 4b.

$$\mu_r(x,y) = \mu_0 \left(1 - \frac{C(x,y)}{C_{max}}\right)^{-2.5 c_{max}} \qquad (10)$$

where $C = (C_{max} - 0.001) \times (1. - y/h)$ was the total supposed sediment concentration and C_{max} a parameter to be chosen.

For this first attempts, in order to explore viscosity influence on the overall results, numerical convergence included, it was supposed that just only the *laminar viscosity* was affected. Fig. 6 shows the dynamical viscosities related to the three selected numerical values *C1*, *C2*, *C3* assumed by the parameter C_{max}, to which different viscosity profiles were associated. Moreover, the fluid density was considered constant (10^3 Kg/m^3) and homogeneous, since the maximum concentration of sediment was assumed equal to about 0.62 Kg/m^3.

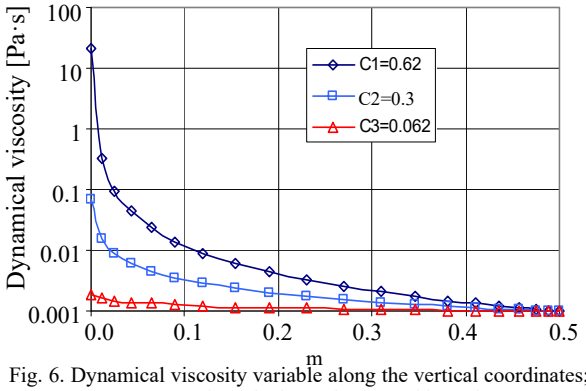

Fig. 6. Dynamical viscosity variable along the vertical coordinates; 0.0 m quote corresponds to the lower horizontal boundary.

In Fig. 7 the effect of spatial variability of viscosity profile on the flow velocity is displayed by the means of a comparison between a laminar flow resulting from constant viscosity and a laminar flow with variable viscosity. It is evident the distortion of the velocity profile (Fig. 7 b). Fig. 8 shows velocity profiles resulting from total boundaries clustering $\alpha = 0.5$, $\beta = 1.15$, turbulent model, different number of iterations and different viscosity profiles.

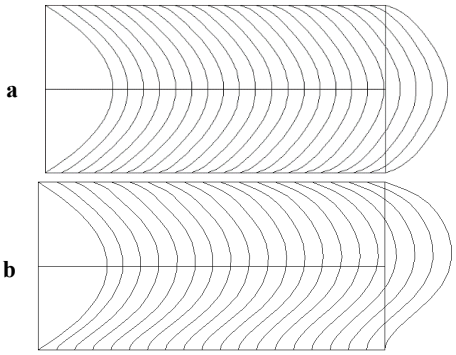

Fig. 7. Poiseuille laminar 3000 iterations, total boundaries clustering: a) clear water $\alpha = 0.5$, $\beta = 1.15$; b) water with variable viscosity due to sediment $\alpha = 0.5$, $\beta = 1.15$.

Finally, convergences of the numerical elaborations related to the velocity and pressure of the turbulent flow, with the three different viscosity profiles, are reported in Fig.9a, b and c, by the means of the residual errors, defined as the following expression, in which $u_x^{(n)}(i)$ and $u_x^{(n-1)}(i)$, are the value of longitudinal velocity of the flow calculated at each node '*i*' and, respectively, at the (*n*)-*th* and the (*n-1*)-*th* iteration [27]:

$$\mathrm{Res(n)} = \sqrt{\sum_{i=1}^{Node}\left[u_x^{(n)}(i) - u_x^{(n-1)}(i)\right]^2 \Big/ \sum_{i=1}^{Node}\left[u_x^{(n)}(i)\right]^2} \qquad (11)$$

As it can be seen from the figure, a better convergence was obtained for higher values of viscosity and for a finer meshing.

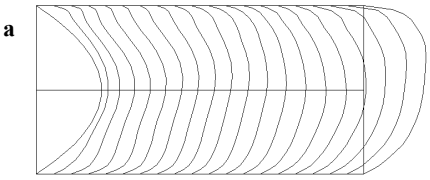

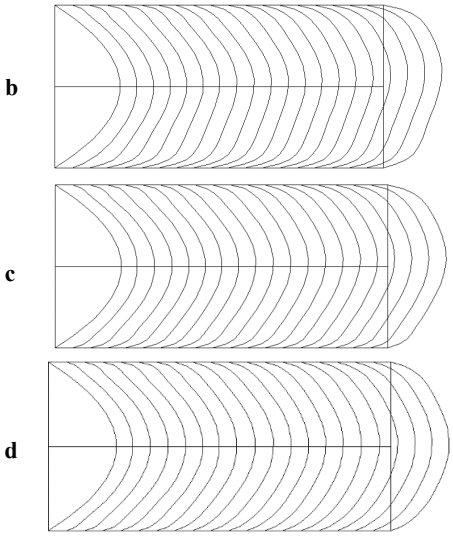

Fig. 8. Turbulent water with variable viscosity, total boundaries clustering: a) 800 iterations C_{max}=C1; b) 2000 iterations C_{max}=C1; c) 2000 iterations C_{max}=C2; d) 2000 iterations C_{max}=C3.

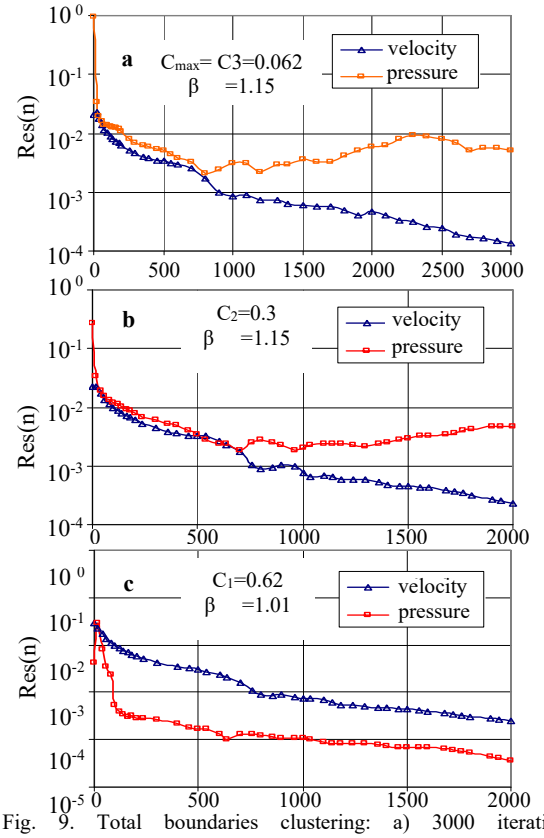

Fig. 9. Total boundaries clustering: a) 3000 iterations, $\alpha = 0.5$, $\beta = 1.15$; b) 2000 iterations, $\alpha = 0.5$, $\beta = 1.15$; c) 2000 iterations, $\alpha = 0.5$, $\beta = 1.01$.

VI. Conclusion

In this paper the influence of an inhomogeneous spatial distribution of sediments through a water flow was explored through simplified assumptions in order to better identify the contributions of selected parameters, also by a numerical point of view, on the developing of the phenomena under

consideration. At this step of the research, the presence of sediments was introduced only through a variable viscosity. Then, the fluid density was considered constant and homogeneous, matching the underlyng assumption that the sediments concentration was low. The tests were based on both laminar and turbulent ($k-\varepsilon$ model) Plane Poiseuille problem, assuming a fixed parabolic longitudinal velocity profile in inlet. A research computer code, already developed and tested by the author [1], based on the CBS-AC stabilization approach, was exploited and further tests were carried out. From the results discussed in this paper, regarding only stationary conditions, the selected algorithms proved to be suitable also to handle spatially variable viscosity, in both laminar and turbulent regime. The spatial variability of the viscosity affects the velocity profiles. The mixing of the momentum and accordingly a redistribution of sediments resulting from turbulence, can significantly affect velocity, sediments density and viscosity profiles in a complex manner. Moreover, the variation of the velocity profile in particular in the vicinity of the banks or of the riverbed can modify the shear stress that induces erosion. However, the study discussed in this paper is a prerequisite to elaborations of the time evolutions of complex phenomenologies. In particular, the study of erosion phenomena and of the resulting mixing, transport and deposition of sediments involve the adoption of iterative procedures with consequent calculation of the velocity field and the feedback on sediment mixing which, in turn, modify velocity spatial profile. Each iteration could be considered as a step towards the stationary state, different in different time, associated to the particular values assumed by the physical parameters characterizing each instant of the transient. Several issues have been not considered, like the impact of the morphology and its change, free surface flows, inclusion of the *Computational Granular Dynamics* and many other ones. The discussion of the results points out the sensitivity of the employed algorithms not only to the mesh size and to their distribution, but also to some intrinsic "experimental dials" (safe coefficients, explicit vs implicit ratio) and to a correct number of iterations, whose knowledge revealed to be fundamental.

REFERENCES

[1] A. Pasculli, 2008. "CFD-FEM 2D Modelling of a local water flow. Some numerical results", *Alpine and Mediterranean Quaternary,* SCOPUS: 2-s2.0-84983037047, 21(B), (1), 215-228.

[2] T.J. Chung, 2006. "*Computational Fluid Dynamics"* Cambridge University Press.

[3] A. Pasculli, N. Sciarra, "A probabilistic approach to determine the local erosion of a watery debris flow", *XI IAEG International Congress*; Liege, Belgium, 3-8 September. SCOPUS id: 2-s2.0-84902449614., Paper S08-08, 2006.

[4] A. Pasculli, A., C. Audisio, 'Cellular Automata Modelling of Fluvial Evolution: Real and Parametric Numerical Results Comparison Along River Pellice (NW Italy)', *Environmental Modeling and Assessment*;. SCOPUS id: 2-s2.0-84940588890, 20, (5), pp. 425-441, 2015.

[5] C. Audisio, A. Pasculli, N. Sciarra, ' Conceptual and numerical models applied on the river pellice (North western italy)', *Engineering Geology for Society and Territory Volume 3,* SCOPUS id: 2-s2.0-84944586202, pp. 327-330, 2015.

[6] A. Pasculli, C. Audisio, G. Lollino, G., 'Application of cellular automaton model for river morphological studies: CAESAR and the Pellice River (Piedmont, Italy)'. *Rendiconti Online Società Geologica Italiana*, SCOPUS id: 2-s2.0-84863090597, 11, (1) pp. 118-119, 2010.

[7] A. Pasculli, C. Audisio, N. Sciarra, 'Water and sediment output evaluation using cellular automata on alpine catchment: Soana, Italy - Test case', *IOP Conference Series: Earth and Environmental Science.* SCOPUS id=2-s2.0-85044335598, 95, pp. 1-8, 2017.

[8] M. Calista, E. Miccadei, A. Pasculli, T. Piacentini, M. Sciarra, N. Sciarra, 2015. "First results of morphometric analysis, multitemporal geomorphological investigation and numerical modeling of the Montebello sul Sangro landslide (Abruzzo, Central Italy)". Rendiconti Online Società Geologica Italiana; Vol. 35, 1 April 2015, pp. 307-310. SCOPUS id: 2-s2.0-84930718363.

[9] M. Calista, E. Miccadei, A. Pasculli, T. Piacentini, M. Sciarra, N. Sciarra, 2016. **"***Geomorphological features of the Montebello sul Sangro large landslide (Abruzzo, Central Italy)*. Journal of Maps. Vol. 12, Issue 5, 19 October 2016, pp. 882-891.; SCOPUS id: 2-s2.0-84944909158.

[10] L. Esposito,A. W. Esposito, A. Pasculli, N. Sciarra, N. 'Particular features of the physical and mechanical characteristics of certain Phlegraean pyroclastic soils'. *CATENA*, SCOPUS id: 2-s2.0-84873130083, 104, pp. 186-194, 2013.

[11] A. Pasculli, N. Sciarra, L. Esposito, A.W. Esposito, **'**Effects of wetting and drying cycles on mechanical properties of pyroclastic soils', *CATENA,* SCOPUS id=2-s2.0-85017109027, 156, 113-123, 2017.

[12] I. Iliopoulos, Y. Mito, T. Hanratty, et al., 2003. "A stochastic model for solid particle dispersion in a nonhomogeneous turbulent field ". Int. J. of Multiphase Flow 29, 375-394.

[13] M. Calista, M., Pasculli, A., Sciarra, N., 2015. **"**Reconstruction of the geotechnical model considering random parameters distributions". Engineering Geology for Society and Territory Volume 2: Landslide processes pp. 1347-1351. SCOPUS id: 2-s2.0-84944628353.

[14] A. Pasculli, L. Minatti, 'Dam break Smoothed Particle Hydrodynamic modeling based on Riemann solvers'. *Advances in Fluid Mechanics VIII, WIT Transactions on Engineering Sciences, WIT Press*, SCOPUS id: 2-s2.0-78449235684, (6) 9, pp. 145-156, 2010.

[15] A. Pasculli, L. Minatti, N. Sciarra, 'Insights on the application of some current SPH approaches for the study of muddy debris flow: Numerical and experimental comparison'. *Wit Transaction 10th International Conference on Advances in Fluid Mechanics, AFM 2014*; A Coruna; Spain, SCOPUS id: 2-s2.0-84907611231, 82, 3–14, 2014.

[16] M.W. Schmeeckle & J.M. Nelson, 2003 –Direct numerical simulation of bedload transport using a local, dynamic boundary condition-Sedimentology, 50, pp. 279-301.

[17] T.I. Zohdi, 2007 Computational of strongly coupled multifield interaction in particle-fluid systems – Comput. Methods Appl. Mech Engrg. 196, pp. 3927-3950.

[18] B.E. Launder, W.P. Jones, 1972 –*Mathematical Models of Turbulence* – Academic Press, New York.

[19] S. Fan, B. Lakshminarayana and M. Barnett, 1993 -Low-Reynolds number $k-\varepsilon$ model for a steady turbulent boundary layers flows-AIAA Journal, 31, pp. 1777-1784.

[20] P. Nithiarasu, R. Codina, O.C. Zienkiewicz, 2006 "*The characteristic Based Split (CBS) scheme* - a unified approach to fluid dynamics". Int. Journal for Numerical Methods in Engineering. 66, 1514-1546.

[21] R. B. Bird & S. Lightfooten, '*Transport Phenomena'* John Wiley & Sons, Inc. New York, pp. 149-161, 1960.

[22] C. Di nucci & E. Fiorucci, 'Mean velocity profiles of fully-developed turbulent flows near smooth walls', *Comptes Rendus Mecanique*, 339, 388-395, 2011.

[23] R. Absi & C. Di Nucci, 'On the accuracy of analytical methods for turbulent flows near smooth walls', *Comptes Rendus Mecanique*, 340, 641-645, 2012.

[24] C. Di nucci & A, Russo Spena, 'Mean velocity profiles of fully-developed turbulent flows', *Comptes Rendus Mecanique*, 340, 629-640, 2012.

[25] C. Di nucci & A, Russo Spena, 'On the steady two-dimensional open channel flow', *Journal of Interdisciplinary Mathematics*, 21 (3), 579–594, 2018.

[26] I.M. Krieger & T.J. Dougherty, 1959. "A mechanism for non-Newton flow in suspension of rigid sphere*"* Trans. Soc. Rheol. 3, pp. 137-152.

[27] O.C. Zienkiewicz, R.L. Taylor & P. Nithiarasu -*Finite Element Method for Fluid Dynamics* - Elsevier, 6thEdition, 2006.